A new model for a drying droplet

S.S. Sazhin[□], O. Rybdylova[□], A.S. Pannala[•], S. Somavarapu[◇], S.K. Zaripov[△]

[□] *Sir Harry Ricardo Laboratories, Advanced Engineering Centre, School of Computing, Engineering and Mathematics, University of Brighton, Brighton, BN2 4GJ, UK*

[•] *Drug Delivery Research Group, School of Pharmacy and Biomolecular Sciences, University of Brighton, Brighton, BN2 4GJ, UK*

[◇] *UCL School of Pharmacy, University College London, 29-39 Brunswick Square, London WC1N 1AX, UK*

[△] *Institute of Environmental Science, Kazan Federal University, Tovarisheskay str, 5, Kazan, 4200097, Russia*

Abstract

A new model for droplet drying is suggested. This model is based on the analytical solutions to the heat transfer and species diffusion equations inside spherical droplets. Small solid particles dispersed in an ambient evaporating liquid, or a non-evaporating substance dissolved in this liquid, are treated as non-evaporating components. Three key sub-processes are involved in the process of droplet drying within the new model: droplet heating/cooling, diffusion of the components inside the droplets, and evaporation of the volatile component. The model is used to analyse the drying of a spray consisting of chitosan dissolved in water. After completion of the evaporation process, the size of the residual solid ball predicted by the model is consistent with those observed experimentally.

Keywords:
Droplets, heating, evaporation, drying, chitosan, water

Nomenclature

$B_{M(T)}$	Spalding mass (heat) transfer number
c	specific heat capacity
D	diffusion coefficient

F	function introduced in Equation (7)
h	convection heat transfer coefficient
h_0	parameter introduced in Equation (2)
h_{0Y}	parameter introduced in Equation (10)
k	thermal conductivity
k_B	Boltzmann constant
L	specific heat of evaporation
Le	Lewes number
M	molar mass
$\dot{m}_d$	evaporation mass rate
Nu	Nusselt number
p	pressure
Pe	Peclet number
Pr	Prandtl number
q_n	parameter introduced in Equation (2)
q_{Yin}	parameter defined by Equation (12)
Q_L	power spent on droplet heating
Q_{Yn}	parameter defined in Equation (11)
R	distance from the droplet centre
R_d	droplet radius
Re	Reynolds number
Sc	Schmidt number
t	time
T^*	normalised temperature
T	temperature
v	velocity
v_n, v_{Yn}	eigenfunctions
V_v	parameter defined in Equation (22)
X	molar fraction
Y	mass fraction

Greek symbols

α	film parameter defined in Equation (9)
ϵ_i	evaporation rate of species i
$\varepsilon_{v(a)}$	characteristic Lennard-Jones energy for vapour (air)
κ_R	parameter introduced in Equation (2)
λ_n	eigenvalues
μ	dynamic viscosity

μ_0	parameter introduced in Equation (2)
ν	kinematic viscosity
ρ	density
σ_v	Lennard-Jones length
χ	coefficient defined in Equation (5)
χ_Y	coefficient defined in Equation (14)
Ω_D	parameter introduced in Equation (24)

Subscripts

air	air
av	average
c	centre
d	droplet
eff	effective
e	evaporation
g	gas
i	species
iso	isolated
l	liquid phase
M	mass transfer
p	constant pressure
r	reference
s	surface, swelling or non-evaporating liquid
total	total
T	heat transfer
v	vapour phase
0	value at the beginning of a time step or initial value
1	value at the end of a time step
∞	ambient

Superscripts

sat	saturated
—	average

1. Introduction

The importance of spray/droplet drying in various engineering and pharmaceutical applications is well known [1, 2, 3, 4]. Spray-drying technology can be utilised to incorporate different excipients as well as active pharmaceutical ingredients into a dry powder formulations. A few advantages include modification of the aerosolisation characteristics of the spray-dried powder [5, 6], and sustained release of the active drug using appropriate modifiers such as hydroxypropyl cellulose [7] and polylactic acid [8]. Reviews of particle engineering via spray drying were presented by Vehring [9] and Yan Wei [10]. Various aspects of, and recent advances in spray drying are presented in [11]. Mezhericher et al. [12] reviewed theoretical studies of slurry droplet evaporation kinetics.

Mathematical models of the evaporation of slurry droplets of various complexity were developed by a number of authors, including [1, 4, 13, 14, 15, 16, 17, 18]. A simplified model for evaporation of slurry droplets was developed by Minoshima et al. [19].

These models have been based on a number of simplifying assumptions, including the assumption that the temperature gradient inside droplets can be ignored. The applicability of these assumptions has not been investigated in most cases. The main aim of this paper is to present the results of the development of a new model for spray drying which relaxes many of the previously used assumptions and takes into account the gradients of small solid particle or dissolved non-evaporating substance concentrations and temperature inside droplets in a self-consistent way.

The new model is based on the model for automotive fuel droplet heating and evaporation, previously developed by one of the authors (SSS) and his colleagues (see [20, 21]). In this model, small solid particles dispersed in an ambient evaporating liquid, or a non-evaporating substance dissolved in this liquid, are treated as non-evaporating components. Analytical solutions to the equations for species diffusion and heat transfer inside droplets are used for the analysis of the process at each time step. The model is applied to the process of spray drying to produce chitosan particles.

Basic equations and assumptions of the model are described in Section 2. The technology involved in the preparation of chitosan particles and input parameters to the model are described in Section 3. The solution algorithm is briefly described in Section 4. Results of calculations, based on the new model and using input parameters described in Section 3, are presented and

discussed in Section 5. The main results of the paper are summarised in Section 6.

2. Model

The model is focused on the analysis of heating and evaporation of droplets with small solid particles dispersed in an ambient evaporating liquid, or a non-evaporating substance dissolved in this liquid. This process eventually leads to the formation of a solid (dry) residue, and the process itself is called drying. As mentioned in the previous section, small solid particles dispersed in an ambient evaporating liquid, or a non-evaporating substance dissolved in this liquid, can be treated as non-evaporating components. This allows us to treat drying droplets as at least bi-component. The droplets are assumed to be perfectly spherical. Three key sub-processes involved in the process of droplet drying will be considered separately in the following sub-sections: droplet heating/cooling, diffusion of the components inside droplets, and evaporation of the volatile component.

2.1. Droplet heating/cooling

The process of droplet heating/cooling is described by the transient heat conduction equation for the temperature $T \equiv T(t, R)$ in the liquid phase, assuming that all processes are spherically symmetric [22, 23]. An analytical solution to this equation, subject to the initial, $T(t = 0) = T_{d0}(R)$, and boundary condition (assuming that the effects of evaporation can be ignored),

$$h(T_g - T_s) = k_{\text{eff}} \left.\frac{\partial T}{\partial R}\right|_{R=R_d-0}, \tag{1}$$

and assuming that the convection heat transfer coefficient $h = \text{const}$, can be presented as [24]:

$$T(R,t) = \frac{1}{R}\sum_{n=1}^{\infty}\left\{q_n \exp\left[-\kappa_R \lambda_n^2 t\right] - \frac{R_d^2 \sin\lambda_n}{||\ v_n\ ||^2\ \lambda_n^2}\mu_0(0)\exp\left[-\kappa_R\lambda_n^2 t\right]\right.$$

$$\left. - \frac{R_d^2 \sin\lambda_n}{||\ v_n\ ||^2\ \lambda_n^2}\int_0^t \frac{\mathrm{d}\mu_0(\tau)}{\mathrm{d}\tau}\exp\left[-\kappa_R\lambda_n^2(t-\tau)\right]\mathrm{d}\tau\right\}\sin\left[\lambda_n\left(\frac{R}{R_d}\right)\right] + T_g(t), \tag{2}$$

where λ_n are solutions to the equation:

$$\lambda \cos \lambda + h_0 \sin \lambda = 0, \tag{3}$$

$$|| \, v_n \, ||^2 = \frac{R_d}{2} \left(1 - \frac{\sin 2\lambda_n}{2\lambda_n} \right) = \frac{R_d}{2} \left(1 + \frac{h_0}{h_0^2 + \lambda_n^2} \right),$$

$$q_n = \frac{1}{|| \, v_n \, ||^2} \int_0^{R_d} \tilde{T}_0(R) \sin \left[\lambda_n \left(\frac{R}{R_d} \right) \right] \mathrm{d}R, \; \kappa_R = \frac{k_{\text{eff}}}{c_l \rho_l R_d^2}, \; \mu_0(t) = \frac{h T_g(t) R_d}{k_{\text{eff}}},$$

$h_0 = (h R_d / k_{\text{eff}}) - 1$, $\tilde{T}_0(R) = R T_{d0}(R)$. The solution to Equation (3) gives a set of positive eigenvalues λ_n numbered in ascending order ($n = 1, 2, ...$). The trivial solution $\lambda = 0$ is not considered. $T_s = T_s(t)$ is the droplet's surface temperature, T_g is the ambient gas temperature (assumed to be constant during the time step), h is linked with the Nusselt number Nu via the equation $\mathrm{Nu} = 2R_d h / k_g$, k_g is the gas thermal conductivity. We assume that vapour is dilute and k_g is equal to the thermal conductivity of air. We are interested only in a solution which is continuously differentiable twice in the whole domain. This implies that T should be bounded for $0 \leq R \leq R_d$. c_l and ρ_l are the specific heat capacity and density, respectively, of the liquid phase, R is the distance from the centre of the droplet, t is time.

Solution (2) is valid for $h_0 > -1$, which is satisfied, remembering the physical background of the problem ($h > 0$). The condition $h = \text{const}$ is valid for sufficiently small time steps.

The derivation of (2) was based on the so called Effective Thermal Conductivity (ETC) model where the effect of droplet motion on the heating/cooling process inside the droplet is taken into account by replacing the liquid thermal conductivity with the effective thermal conductivity k_{eff}. k_{eff} is linked with the liquid thermal conductivity k_l via the following equation:

$$k_{\text{eff}} = \chi k_l, \tag{4}$$

where the coefficient χ can be approximated as [26]:

$$\chi = 1.86 + 0.86 \tanh \left[2.245 \log_{10} \left(\mathrm{Pe}_{d(l)} / 30 \right) \right], \tag{5}$$

$\mathrm{Pe}_{d(l)} = \mathrm{Re}_{d(l)} \mathrm{Pr}_l$ is the liquid Peclet number. Liquid fuel transport properties and the liquid velocity just below the droplet surface (see [26] for details) were used to calculate $\mathrm{Pe}_{d(l)}$.

Note that in some papers and books, including [20], coefficient 2.225 is used in Formula (5) instead of 2.245. Our analysis is based on the formula originally suggested in [26].

The effect of droplet evaporation in analytical solution (2) is taken into account by replacing gas temperature with the so-called effective temperature defined as:

$$T_{\text{eff}} = T_g + \frac{\rho_l L \dot{R}_{de}}{h}, \tag{6}$$

where L is the latent heat of evaporation, $\dot{R}_{de}$ is the change in droplet radius due to evaporation, which is taken from the previous time step and estimated based on Equation (19). R_d and all other thermodynamic and transport properties are assumed constant in the analytical solution, but are updated at the end of each time step Δt. The effects of non-constant droplet radius during the droplet heating process were discussed in [20], and will not be taken into account in our analysis.

In the limit $k_{\text{eff}} \to \infty$ the prediction of Expression (2) reduces to the one which follows from the model based on the assumption that $k_{\text{eff}} = \infty$ [25] (Infinite Thermal Conductivity (ITC) model). The value of Nu for an isolated moving droplet is estimated based on the following equation [26]:

$$\text{Nu}_{\text{iso}} = 2\frac{\ln(1+B_T)}{B_T}\left(1 + \frac{(1+\text{Re}_d\text{Pr}_d)^{1/3}\max\left[1,\text{Re}_d^{0.077}\right]-1}{2F(B_T)}\right), \tag{7}$$

where $B_T = \frac{c_{pv}(T_g - T_s)}{L_{\text{eff}}}$ is the Spalding heat transfer number,

$$F(B_T) = (1+B_T)^{0.7}\frac{\ln(1+B_T)}{B_T}, \;\; L_{\text{eff}} = L + \frac{Q_L}{\dot{m}_d} = \sum_i \epsilon_i L_i + \frac{Q_L}{\sum_i \dot{m}_i},$$

Q_L is the power spent on droplet heating, c_{pv} is the specific heat capacity of fuel vapour, $\epsilon_i = \epsilon_i(t)$ are the evaporation rates of species i, defined in Equation (15), $\dot{m}_i = \epsilon_i \dot{m}_d$ ($\dot{m}_d = \sum_i \dot{m}_i$). The effects of the interaction between droplets are ignored (simplified models for these effects are discussed in [27, 28]).

2.2. Species diffusion in the liquid phase

As mentioned earlier, our analysis is focused on bi-component droplets, with one non-evaporating component. The diffusion of both evaporating and non-evaporating components inside a spherical droplet is described by a well

known species diffusion equation [20, 30]. The analytical solution to this equation was obtained subject to the following boundary condition [29]:

$$\alpha(\epsilon_i - Y_{lis}) = -D_{\text{eff}} \left.\frac{\partial Y_{li}}{\partial R}\right|_{R=R_d-0}, \tag{8}$$

and the initial condition $Y_{li}(t=0) = Y_{li0}(R)$, where $Y_{lis} = Y_{lis}(t)$ are liquid or non-evaporating components' mass fractions at the droplet's surface ($i = 1, 2$),

$$\alpha = \frac{|\dot{m}_d|}{4\pi\rho_l R_d^2}, \tag{9}$$

$\dot{m}_d$ is the droplet evaporation rate, the calculation of which is discussed in the next sub-section (see Equation (17)). As in the case of the heat conduction equation, we are interested only in a solution which is continuously differentiable twice in the whole domain. This implies that Y_{li} should be bounded for $0 \le R \le R_d$. This led to the following expression for Y_{li} [29]:

$$Y_{li} = \epsilon_i + \frac{1}{R}\left\{\exp\left[D_{\text{eff}}\left(\frac{\lambda_0}{R_d}\right)^2 t\right][q_{Yi0} - Q_{Y0}\epsilon_i]\sinh\left(\lambda_0\frac{R}{R_d}\right)\right.$$

$$\left. + \sum_{n=1}^{\infty}\left[\exp\left[-D_{\text{eff}}\left(\frac{\lambda_n}{R_d}\right)^2 t\right][q_{Yin} - Q_{Yn}\epsilon_i]\sin\left(\lambda_n\frac{R}{R_d}\right)\right]\right\}, \tag{10}$$

where λ_0 and λ_n ($n \ge 1$) are solutions to the equations

$$\tanh\lambda_0 = -\frac{\lambda_0}{h_{0Y}} \quad \text{and} \quad \tan\lambda_n = -\frac{\lambda_n}{h_{0Y}} \ \ (n \ge 1),$$

respectively, $h_{0Y} = -\left(1 + \frac{\alpha R_d}{D_{\text{eff}}}\right)$,

$$Q_{Yn} = \begin{cases} -\frac{1}{||v_{Y0}||^2}\left(\frac{R_d}{\lambda_0}\right)^2(1+h_{0Y})\sinh\lambda_0 & \text{when} \quad n=0 \\ \frac{1}{||v_{Yn}||^2}\left(\frac{R_d}{\lambda_n}\right)^2(1+h_{0Y})\sin\lambda_n & \text{when} \quad n\ge 1 \end{cases} \tag{11}$$

$$q_{Yin} = \frac{1}{||v_{Yn}||^2}\int_0^{R_d} R Y_{li0}(R) v_n(R)\mathrm{d}R, \tag{12}$$

$n \ge 0$,

$$v_{Y0}(R) = \sinh\left(\lambda_0\frac{R}{R_d}\right), \quad v_{Yn}(R) = \sin\left(\lambda_n\frac{R}{R_d}\right), \ \ n \ge 1.$$

D_{eff} is linked with the liquid diffusivity D_l via the following equation

$$D_{\text{eff}} = \chi_Y D_l, \tag{13}$$

where the coefficient χ_Y can be approximated as:

$$\chi_Y = 1.86 + 0.86 \tanh\left[2.225 \log_{10}\left(\text{Re}_{d(l)}\text{Sc}_l/30\right)\right], \tag{14}$$

$\text{Sc}_l = \nu_l/D_l$ is the liquid Schmidt number, ν_l is the liquid kinematic viscosity. As in the case of k_{eff}, liquid fuel transport properties and the liquid velocity just below the droplet surface were used to calculate $\text{Re}_{d(l)}$. The model based on Equations (13) and (14) is known as the Effective Diffusivity (ED) model. The model based on the assumption that species diffusivity is infinitely fast ($D_{\text{eff}} = \infty$) is referred to as the Infinite Diffusivity (ID) model. The estimation of D_l is discussed later. The combined ITC/ID model is sometimes known as a well-mixed model.

The values of ϵ_i can be found from the following relationship [29]:

$$\epsilon_i = \frac{Y_{vis}}{\sum_i Y_{vis}}, \tag{15}$$

where the subscript $_v$ indicates the vapour phase.

This model is applied to the problem of drying in which a suspension of small particles or dissolved non-evaporating substance is treated as a non-evaporating liquid ($i = s$) mixed with an evaporating liquid ($i = l$). In this case: $\epsilon_l = 1$ and $\epsilon_s = 0$. Partial pressure of the evaporating liquid at the surface of the droplet is estimated from Raoult's law as

$$p_v = X_{ls} p_v^{\text{sat}}, \tag{16}$$

where X_{ls} is the molar fraction of liquid just below the droplet surface, p_v^{sat} is the saturated pressure of vapour.

We do not see any limitations to the application of this approach to the analysis of heating and evaporation of liquid droplets with a dissolved non-evaporating substance, provided that the diffusion coefficient between the liquid and the non-evaporating substance can be specified. In the case of suspension of small particles in a liquid this approach is applicable only when the number of suspended particles is sufficiently large to ensure the applicability of diffusion theory to the analysis of particle motion.

2.3. Droplet evaporation

The evaporation rate of isolated mono-component droplets is estimated as [20, 26, 30]:

$$\dot{m}_d = -2\pi R_d D_v \rho_{\text{total}} B_M \text{Sh}_{\text{iso}}, \tag{17}$$

where D_v is the binary diffusion coefficient of vapour in air, B_M is the Spalding mass transfer number defined as:

$$B_M = \frac{\rho_{vs} - \rho_{v\infty}}{\rho_{gs}} = \frac{Y_{vs} - Y_{v\infty}}{1 - Y_{vs}}, \tag{18}$$

ρ_{vs} and Y_{vs} are vapour density and mass fraction at the surface of the droplet estimated from the ideal gas law and Equation (16) (mass fractions and partial pressures are linked by Equation (4.9) of [20]), Sh_{iso} is the Sherwood number approximated following [30].

The derivation of Equation (17) is essentially based on the assumption that ρ_{total} remains the same at all distances from the droplet surface. This assumption was relaxed in the recently developed model described by Tonini and Cossali (see [20, 21]).

When calculating the value of $\dot{R}_d$ we took into account both droplet evaporation and the change in droplet density due to temperature (swelling/contraction) during the time step (see Equation (20) in [36]):

$$\dot{R}_d = \dot{R}_{de} + \dot{R}_{ds}, \tag{19}$$

where $\dot{R}_{de}$ and $\dot{R}_{ds}$ are the rates of change of droplet radii due to evaporation and swelling/contraction defined as

$$\dot{R}_{de} = \frac{\dot{m}_d}{4\pi R_d^2 \rho_l}, \quad \dot{R}_{ds} = \frac{R_d(\overline{T}_0)}{\Delta t}\left[\left(\frac{\rho(\overline{T}_0)}{\rho(\overline{T}_1)}\right)^{1/3} - 1\right],$$

$\overline{T}_0$ and $\overline{T}_1$ are average droplet temperatures at the beginning $t = t_0$ and the end of the time step $t = t_1$, $\Delta t = t_1 - t_0$.

2.4. Liquid diffusion coefficient

Our analysis is based on the assumption that dissolved non-evaporating substances can be treated similarly to non-dissolved substances with masses

of particles equal to molecular masses. This allows us to estimate the liquid diffusion coefficient based on the Wilke-Chang formula [33]:

$$D_l = \frac{7.4 \times 10^{-15} \sqrt{\overline{M}_v} T}{\mu_l V_v^{0.6}}, \tag{20}$$

where $\overline{M}_v$ is the average molar mass defined as

$$\overline{M}_v = \left[\sum_{i=1}^{i=2} \left(Y_i / M_i \right) \right]^{-1}, \tag{21}$$

$i = 1 = l$ refers to liquid, while $i = 2 = s$ refers to solid particles or dissolved non-evaporating matter,

$$V_v = \left(\sigma_v / 1.18 \right)^3, \tag{22}$$

σ_v is the Lennard-Jones length (in Å) estimated as [20, 34]:

$$\sigma_v = 1.468 \, \overline{M}_v^{0.297}, \tag{23}$$

where $\overline{M}_v$ is the average molar mass (in kg/kmole), estimated based on (21).

2.5. Vapour diffusion coefficient

Assuming that the evaporating liquid is water, and the evaporation takes place in air, the average diffusion coefficient is estimated from the Wilke and Lee formula [32]:

$$D_{va} = \frac{\left[3.03 - \left(0.98 / M_{va}^{1/2} \right) \right] (10^{-7}) T^{3/2}}{p M_{va}^{1/2} \sigma_{va}^2 \Omega_D}, \tag{24}$$

where D_{va} is in m^2/s, T is temperature in K,

$$M_{va} = 2 \left[(1/M_w) + (1/M_a) \right]^{-1},$$

M_w and M_a are molar masses of water and air, p is pressure in bar, $\sigma_{va} = (\sigma_w + \sigma_a)/2$, σ_w and σ_a are characteristic Lennard-Jones lengths for water vapour and air respectively, measured in Angstrom (Å) (see Equation (23)), Ω_D is the function of the normalised temperature $T^* = k_B T / \varepsilon_{va}$, $\varepsilon_{va} = \sqrt{\varepsilon_v \, \varepsilon_a}$, ε_v and ε_a are characteristic Lennard-Jones energies for vapour and air

respectively, k_B is the Boltzmann constant. Ω_D is a relatively weak function of $\varepsilon_v/k_B = 97$ K (see Tables E.1 and E.2 of [33]).

All liquid properties are calculated for average temperatures inside droplets. All gas properties are calculated for the reference temperature $T_r = (2/3)T_s + (1/3)T_g$, where T_s and T_g are droplet surface and ambient gas temperatures, respectively. Enthalpy of evaporation and saturated vapour pressure are estimated at the surface temperature T_s.

2.6. Average values of properties

The average values of liquid density and specific heat capacity taking into account the contributions of both components are estimated using the following formulae [32, 36]:

$$\overline{\rho}_l = \left[\sum_{i=1}^{i=2} \left(Y_i / \rho_{li} \right) \right]^{-1}, \tag{25}$$

$$\overline{c}_l = \sum_{i=1}^{i=2} \left(Y_i c_{li} \right), \tag{26}$$

Following [37], liquid viscosity is estimated as:

$$\ln \overline{\mu}_l = \sum_{i=1}^{i=2} X_i \ln \mu_{li}, \tag{27}$$

where μ_{li} are dynamic viscosities of liquid components.

Also, following [37], liquid thermal conductivity is estimated as:

$$\overline{k}_l = \left(\sum_{i=1}^{i=2} Y_i k_{li}^{-2} \right)^{-1/2}, \tag{28}$$

where k_{li} are thermal conductivities of liquid components.

Strictly speaking Formula (28) is valid only when the ratios of thermal conductivity of components do not exceed two, but this limitation is not expected to affect the results significantly as during most of the evaporation process the mass fraction of water is expected to be much larger than that of suspended particles.

3. Description of the experiment and input parameters

3.1. Preparation of chitosan particles by spray drying

Chitosan was weighed on a high accuracy analytical balance (SD ±0.2 mg) and dissolved in de-ionized water. The resultant solution was spray-dried using a lab-scale nanospray dryer, Büchi B-90 (Büchi Labortechnik AG, Switzerland), equipped with a piezoelectrically driven droplet atomizing technology [38]. The spray drying was carried out using a pump flow rate of 20 mL/h with a gas flow rate of 133 L/min and an inlet temperature of 120°C. The sample was aspired at 100% through a 5.5 μm mesh nozzle with an instrument pressure of 47 mbar. In order to avoid crystallization, the spray dried powders were immediately transferred into a closed glass vial and stored in a desiccator.

The shape and surface morphology of the spray-dried chitosan powder was investigated using scanning electron microscopy (SEM) (FEI Quanta 200F SEM; Eindhoven, Netherlands). Spray-dried samples were placed on aluminium stubs (Agor Scientific, UK) and sputter coated with gold (Quorum Q150R; Quorum Technologies Ltd., UK) prior to observation under SEM.

Particle size of the spray-dried powder nanoparticles was determined using a Sympatec HELOS/RODOS BF laser diffractor (Sympatec GmbH, Clausthal-Zellerfeld, Germany). An aliquot of the spray-dried sample was loaded into the u-shaped tube to cover a length of approximately 1 cm. The tube was then inserted into the device (ASPIROS) and the sample was analysed at an air pressure of 4 bar. The spray-dried sample was analysed in triplicate. The particle size distribution range was calculated and analysed using WINDOX 5.0 software.

Our analysis will focus on the modelling of drying water droplets containing dissolved polymer (chitosan).

3.2. Multiphase flow

Droplets were created from a solution of 0.2 g polymer in 50 g water [39]. Thus the initial mass fraction of the polymer (Y_{p0}) in the droplets was 4×10^{-3}=0.004 and the initial mass fraction of water (Y_{w0}) was 0.996.

The drying gas volume flow rate was 133 L/min, blown through a drying chamber of cross sectional area 0.23758 m^2 (pipe diameter 0.55 m). Thus the average flow velocity was 9.33×10^{-3} m/s. The drying gas was at atmospheric pressure and had a temperature of 120°C=393 K.

Scanning electron microscopy (SEM) was used to determine the surface morphology, structural characteristics and visual particle sizes. A typical SEM micrograph for the spray-dried chitosan particles is shown in Figure 1. It can be seen from the figure that the surfaces of some of the particles have a dimpled appearance. This observation has previously been reported for chitosan-levofloxacin and leucine-levofloxacin nanoparticles [38].

Particle size analysis of the spray-dried chitosan powder, as determined by laser diffraction (Sympatec), found particles in the range 1 μm to 3.2 μm. This range is similar to the size distribution inferred from the SEM analysis. These observations are also in agreement with the predicted size distribution as discussed later.

It is not easy to estimate the average velocities of droplets relative to the ambient gas. We can expect, however, that except in the immediate vicinity of the nozzle this velocity is very low and we can ignore its contribution to the heat/mass transfer process altogether [20].

The average initial droplet diameters were assumed to be equal to 20 μm [39]; the droplets were supplied at room temperature, assumed equal to 293 K.

3.3. Transport and thermodynamic properties of components

Assuming that the density of chitosan is similar to that of cellulose acetate, a value of 1300 kg/m^3 for polymer density was used in our analysis. Its temperature dependence in the range of temperatures 293 K – 393 K was ignored. The temperature dependence of the density of water could be approximated based on data presented in Table A.6 of [41], but in our case it was assumed to be constant at 945.2 kg/m^3. The swelling of droplets is not considered at this stage (this effect is not expected to be important).

Assuming that the specific heat capacity of chitosan is similar to that of cellulose acetate, a value of 0.4 cal/(g °C)= 1.6747 kJ/(kg K)[1] was used in our analysis. The temperature dependence of the specific heat capacity of water could be approximated based on data presented in Table A.6 of [41]. In our case, data provided in [43] were used.

Assuming that the thermal conductivity of chitosan is similar to that of cellulose acetate, a value of 0.25 W/(m K)[2] was used in our analysis. The

[1]The following range of heat capacities was recommended in [40]: 0.3 – 0.5 cal/(g °C).

[2]The following range of thermal conductivities was recommended in [40]: 0.17 – 0.33 W/(m K).

temperature dependence of the thermal conductivity of water could be based on data presented in Table A.6 of [41]. In our case, data provided in [43] were used.

The temperature dependence of saturated water vapour pressure could be approximated based on data presented in Table A.6 of [41]. In our case, data provided in [43] were used. The saturated vapour pressure of the polymer is assumed equal to zero for all temperatures under consideration.

The polymer is assumed to remain solid in the temperature range under consideration (under 100 °C) [42]. The average molar mass of polymer dissolved in water is assumed to be equal to 120,000 kg/kmole.[3] The liquid diffusion coefficient and thermal conductivity were calculated based on Formulae (20) and (28), respectively, remembering that the molar mass of water is equal to 18 kg/kmole.

The viscosity of the mixture of water and polymer is assumed to be the same as that of water. The temperature dependence of the viscosity of water was approximated based on data presented in Table A.6 of [41].

4. Solution algorithm

These are the main steps of the numerical algorithm:

1. Assume the initial distribution of temperature and mass fractions of species across the droplet, or use the distributions obtained at the previous time step (in our case all initial distributions are assumed homogeneous).

2. Calculate water partial pressure and molar fraction in the gas phase using Equation (16).

3. Calculate the value of the water evaporation rate (ϵ_l) using Equation (15).

4. Calculate the values of liquid thermal conductivity and other properties for the mixture of species.

5. Calculate the distribution of temperature inside the droplet based on Equation (2), using 100 terms in the series.

6. Calculate the distribution of species inside the droplet based on Equation (10), using 200 terms in the series.

7. Calculate the change in droplet size using Equation (19); recalculate the droplet size at the end of the time step.

[3]The actual range of molar masses was 50,000 to 190,000 kg/kmole.

8. Return to Step 1 and repeat the calculations for the next time step.

The results were obtained using discretisation into 500 cells in the droplet radial direction.

5. Results

The plot of droplet radius versus time is shown in Figure 2. As follows from this figure, a conventional droplet evaporation process can be observed until approximately $t = 0.127$ s. After this time, the evaporation process stops and the droplet turns into a solid polymer ball of radius 1.51 μm. This radius is approximately 6% larger than one would expect based on the initial mass of chitosan in the droplet. At present, the reason for this deviation is not fully understood, but the problems associated with calculating highly accurate droplet radii at the final stages of droplet heating and evaporation are well known [20].

The plots of droplet central, average and surface temperatures versus time are shown in Figure 3. As follows from this figure, the gradual increase in all three temperatures with time until approximately $t = 0.127$ s is consistent with predictions of the behaviour of these temperatures for similar heated and evaporating droplets [20]. A sharp increase in these temperatures after approximately $t = 0.127$ s is attributed to the fact that the evaporation process stops at this time and all energy supplied to the solid ball is spent on its heating.

The plots of water and chitosan surface mass fractions versus time are shown in Figure 4. As follows from this figure, the contribution of chitosan in the mixture can be considered negligibly small at t less than about 0.1 s. At times greater than 0.12 s, however, the mass fractions of these substances become comparable, and at times close to 0.127 s, the mass fraction of chitosan becomes larger than that of water. These properties of the mass fractions are consistent with the results shown in Figures 2 and 3.

The predicted radius of the polymer ball (1.51 μm) lies in the range of radii observed in the experiments as discussed in Section 3 (Figure 1). It is thought that the smaller and larger balls are produced by smaller and larger droplets not considered in our calculations.

It is not easy to compare the evaporation time of droplets predicted by our model (about 0.13 s) with the ones observed experimentally. The actually observed spray is polydispersed and the interaction between droplets plays a crucial role in the process. Both effects are ignored in our analysis. We

can, however, estimate the fastest possible drying time of droplets as the ratio of the radius of the drying chamber (0.28 m) to the fastest droplet velocity (v_d). The latter can be estimated as the ratio of the liquid flow rate (20 mL/h) to the area of a nozzle with diameter 5.5 μm. This led us to a maximal velocity of 23 m/s and a minimum droplet evaporation time of 0.012 s, which is an order of magnitude lower than predicted by the model. Since the actual velocity of droplets in the chamber is expected to be about an order of magnitude lower than this value (see [20]), we can conclude that the predictions of the model do not contradict experimental data.

6. Conclusions

A new model for droplet drying based on analytical solutions to the heat transfer and species diffusion equations inside droplets is suggested. Small solid particles dispersed in an ambient evaporating liquid, or a non-evaporating substance dissolved in this liquid, are treated as non-evaporating components. The droplets are assumed to be spherical. Three key sub-processes are involved in the process of droplet drying within the new model: droplet heating/cooling, diffusion of the components inside droplets, and evaporation of the volatile component.

The model is used to analyse the drying of a droplet which consists of chitosan dissolved in water using the experimental data described in [38]. Assuming that the initial droplet radius is equal to 10 μm, gas temperature equal to 393 K and the initial mass fractions of chitosan and water are equal to 0.004 and 0.996, respectively, plots of the time evolution of droplet radius, temperatures and mass fractions of the components were prepared. It is pointed out that the evaporation process is completed by about $t = 0.127$ s, when a droplet turns into a solid ball of radius 1.51 μm. The size of this ball is consistent with those observed experimentally.

Acknowledgements

The authors are grateful to the EPSRC (UK) (Grants EP/M002608/1 and EP/R012024/1), the Royal Society (UK), and the Russian Foundation for Basic Research (Grant No. 16-51-10024) for their financial support. The UK Fluids network is gratefully acknowledged for its support of the Special Interest Group 'Sprays in engineering applications: modelling and experimental studies'. This group was used as a platform for the exchange of ideas

between researchers working on various aspects of spray research. This paper originated as a results of this exchange of ideas.

References

[1] Vehring R, Foss WR, Lechuga-Ballesteros D. Particle formation in spray drying. Journal of Aerosol Science 2007;38:728-746.

[2] Zhu Y-Y, Guo Y, Wang C-Y, Qiao Z-J, Chen M-M. Fabrication of conductive carbonaceous spherical architecture from pitch by spray drying. Chemical Engineering Science 2015;135:109-116.

[3] Singh A, Van den Mooter G. Spray drying formulation of amorphous solid dispersions. Advanced Drug Delivery Reviews 2016;100:27-50.

[4] Porowska A, Dosta M, Fries L, Gianfrancesco A, Heinrich S, Palzer S. Predicting the surface composition of a spray-dried particle by modelling component reorganization in a drying droplet. Chemical Engineering Research and Design 2016;110:131-140.

[5] Rabbani NR, Seville PC. The influence of formulation components on the aerosolisation properties of spray-dried powders. Journal of Controlled Release 2005;110:130-140.

[6] Li HY, Neill H, Innocent R, Seville P, Williamson I, Birchall JC. Enhanced dispersibility and deposition of spray-dried powders for pulmonary gene therapy. Journal of Drug Targeting 2003;11:425-432.

[7] Surendrakumar K, Martyn GP, Hodgers EC, Hansen M, Blair JA. Sustained release of insulin from sodium hyaluronate based dry powder formulations after pulmonary delivery to beagle dogs. Journal of Controlled Release 2003;91:385-94.

[8] Taylor MK, Hickey AJ, Vanroot M. Manufacture, characterization, and pharmacodynamic evaluation of engineered ipratropium bromide particles. Pharmaceutical Development and Technology 2006;11:321-336.

[9] Vehring R. Pharmaceutical particle engineering via spray drying. Pharmaceutical Research 2008;25(5):999-1022.

[10] Yan Wei. Effect of particles on evaporation of droplet containing particles. Doctoral Dissertation (Open Access), Electronic Theses and Dissertations. Paper 731. University of Central Florida 2015.

[11] Paudel A , Worku ZA, Meeus J, Guns S, Mooter GV. Manufacturing of solid dispersions of poorly water soluble drugs by spray drying: Formulation and process considerations. International Journal of Pharmaceutics 2013;453(30):253-284.

[12] Mezhericher M, Levy A, Borde I. Theoretical models of single droplet drying kinetics: a review. Drying Technology 2010;28 (2),278-293.

[13] Cheong HW, Jeffreys GV, Mumford, CJ. A receding interface model for the drying of slurry droplets. AIChE Journal 1986;32(8),1334-1346.

[14] Lee A, Law CK. Gasification and shell characteristics in slurry droplet burning. Combustion and Flame 1991;85(1):77-93.

[15] Nesic S, Vodnik J. Kinetics of droplet evaporation. Chemical Engineering Science 1991;46(2):527-537.

[16] Levi-Hevroni D, Levy A, Borde I. Mathematical modeling of drying of liquid or solid slurries in steady state one-dimensional flow. Drying Technology 1995;13(5-7):1187-201.

[17] Mezhericher M, Levy A, Borde I. Theoretical drying model of single droplets containing insoluble or dissolved solids. Drying Technology 2007;25(6):1025-1032.

[18] Dalmaz N, Ozbelge N, Eraslan HO, Uludag Y. Heat and mass transfer mechanisms in drying of a suspension droplet: a new computational model. Drying Technology 2007;25(2):391-400.

[19] Minoshima H, Matsushima K, Liang H, Shinohara K. Basic model of spray drying granulation. Journal of Chemical Engineering of Japan 2001;34(4):472-478.

[20] Sazhin SS. Droplets and Sprays. Springer, 2014. ISBN: 978-1-4471-6385-5.

[21] Sazhin SS Modelling of fuel droplet heating and evaporation: recent results and unsolved problems, Fuel 2017;196:69-101. DOI: http://dx.doi.org/10.1016/j.fuel.2017.01.048.

[22] Carslaw HS, Jaeger JC. Conduction of Heat in Solids. Second Edition. Oxford: Clarendon Press, 1986.

[23] Kartashov EM. Analytical Methods in Heat Transfer Theory in Solids. Moscow: Vysshaya Shkola; 2001 (in Russian).

[24] Sazhin SS, Krutitskii PA, Abdelghaffar WA, Mikhalovsky SV, Meikle ST, Heikal MR. Transient heating of diesel fuel droplets. International Journal of Heat and Mass Transfer 2004;47:3327-3340.

[25] Sazhin SS, Krutitskii PA. A conduction model for transient heating of fuel droplets. In Begehre HGW, Gilbert RP, Wong MW, editors. Progress in Analysis Vol. II. Proceedings of the 3rd International ISAAC (International Society for Analysis, Applications and Computations) Congress (August 20 - 25, 2001, Berlin), Singapore: World Scientific; pp. 1231-1239; 2003.

[26] Abramzon B, Sirignano WA. Droplet vaporization model for spray combustion calculations. International Journal of Heat and Mass Transfer 1989;32:1605-1618.

[27] Maqua C, Castanet G, Grisch F, Lemoine F, Kristyadi T, Sazhin SS. Monodisperse droplet heating and evaporation: experimental study and modelling. International Journal of Heat and Mass Transfer 2008;51:3932-3945.

[28] Sazhin SS, Elwardany AE, Krutitskii PA, Deprédurand V, Castanet G, Lemoine F, Sazhina EM, Heikal MR. Multi-component droplet heating and evaporation: numerical simulation versus experimental data. International Journal of Thermal Science 2011;50:1164-1180.

[29] Sazhin SS, Elwardany AE, Krutitskii PA, Castanet G, Lemoine F, Sazhina EM, Heikal MR. A simplified model for bi-component droplet heating and evaporation. International Journal of Heat and Mass Transfer 2010;53:4495-44505.

[30] Sazhin SS. Advanced models of fuel droplet heating and evaporation. Progress in Energy and Combustion Science 2006;32:162-214.

[31] Elwardany AE, Gusev IG, Castanet G, Lemoine F, Sazhin SS. Mono- and multi-component droplet cooling/heating and evaporation: comparative analysis of numerical models. Atomization and Sprays 2011;21:907-931.

[32] Poling BE, Prausnitz JM, O'Connell J. The Properties of Gases and Liquids. 5th Edition. New York: McGraw-Hill, 2001.

[33] Bird RB, Stewart EW, Lightfoot EN. Transport Phenomena. Second Edition. New York, Chichester: Wiley & Sons, 2002.

[34] Silva CM, Li H, Macedo EA. Models for self-diffusion coefficients of dense fluids, including hydrogen-bonding substances. Chemical Engineering Science 1998;53:2423-2429.

[35] Abramzon B, Sazhin SS. (2006) Convective vaporization of fuel droplets with thermal radiation absorption. Fuel 2006;85:32-46.

[36] Sazhin SS, Al Qubeissi M, Kolodnytska R, Elwardany A, Nasiri R, Heikal MR. Modelling of biodiesel fuel droplet heating and evaporation, Fuel 2014;115:559-572.

[37] Sazhin SS, Al Qubeissi M, Nasiri R, Gun'ko VM, Elwardany AE, Lemoine F, Grisch F, Heikal MR. A multi-dimensional quasi-discrete model for the analysis of Diesel fuel droplet heating and evaporation. Fuel 2014;129:238-266.

[38] Anandharamakrishnan, C., Padma Ishwarya S. Spray Drying Techniques for Food Ingredient Encapsulation. John Wiley & Sons, UK, Chapter 1, pages 1-36, 2015.

[39] Merchant Z, Taylor KMG, Stapleton P, Razak SA, Kunda N, Alfagih I, Sheikh K, Saleem IY, Somavarapu S. Engineering hydrophobically modified chitosan for enhancing the dispersion of respirable microparticles of levofloxacin. European Journal of Pharmaceutics and Biopharmaceutics 2014;88:816-829.

[40] www.engineeringtoolbox.com

[41] Incropera FP, DeWitt DP. Introduction to Heat Transfer. Fourth Edition: John Wiley & Sons, 2002.

[42] www.sigma-aldrich.co.uk

[43] Yaws, CL. Thermophysical Properties of Chemicals and Hydrocarbons. William Andrew, 2008.

Figure Captions

Figure 1 A typical SEM micrograph for spray-dried chitosan particles.

Figure 2 Droplet radius (in μm) versus time for input parameters described in Section 3.2.

Figure 3 Droplet central, average and surface temperatures versus time for input parameters described in Section 3.2.

Figure 4 Water and chitosan surface mass fractions versus time for input parameters described in Section 3.2.

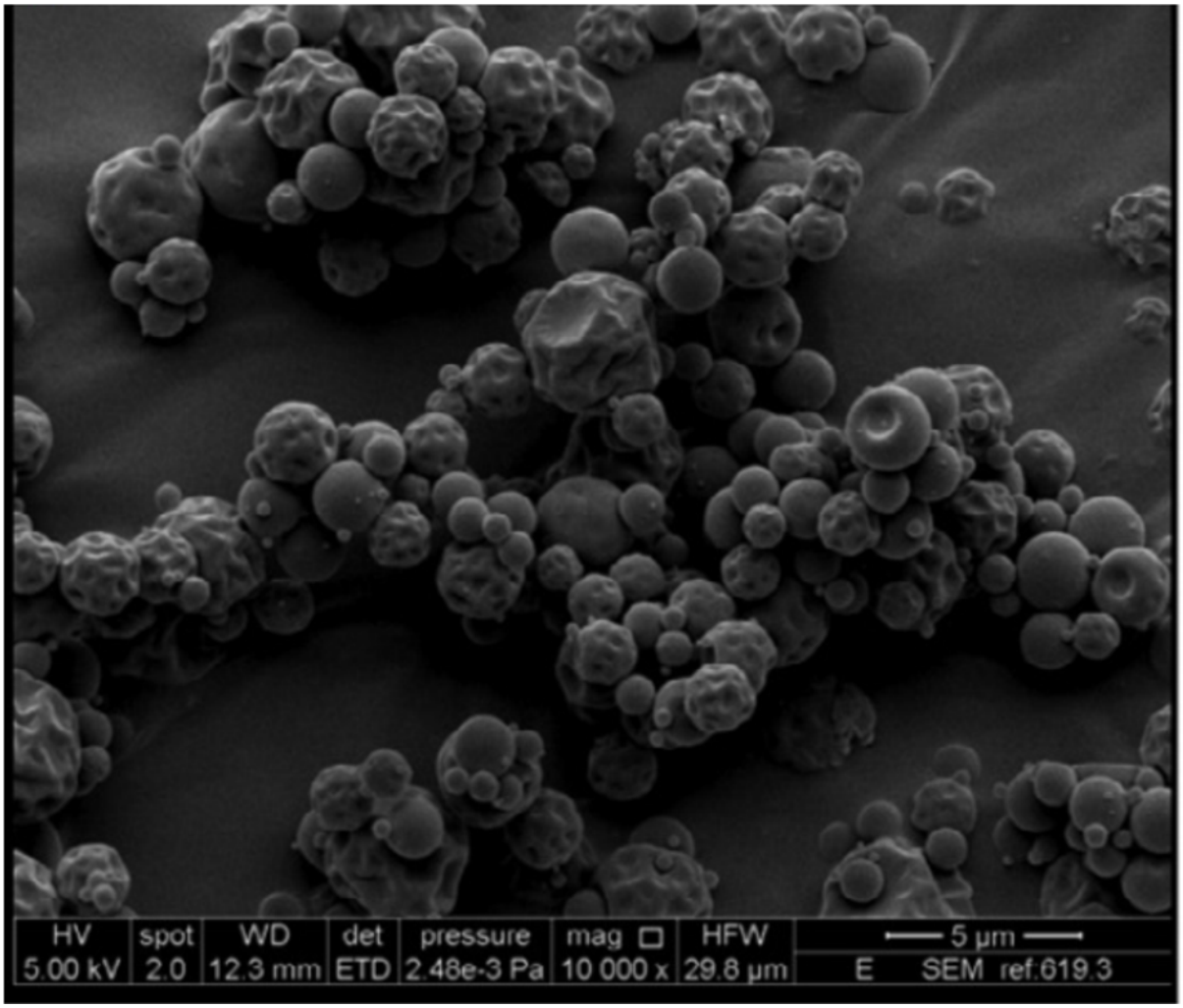
HV
5.00 kV
spot
2.0
WD
12.3 mm
det
ETD
pressure
2.48e-3 Pa
mag
10 000 x
HFW
29.8 µm
5 µm
E
SEM ref.619.3

Figure 1

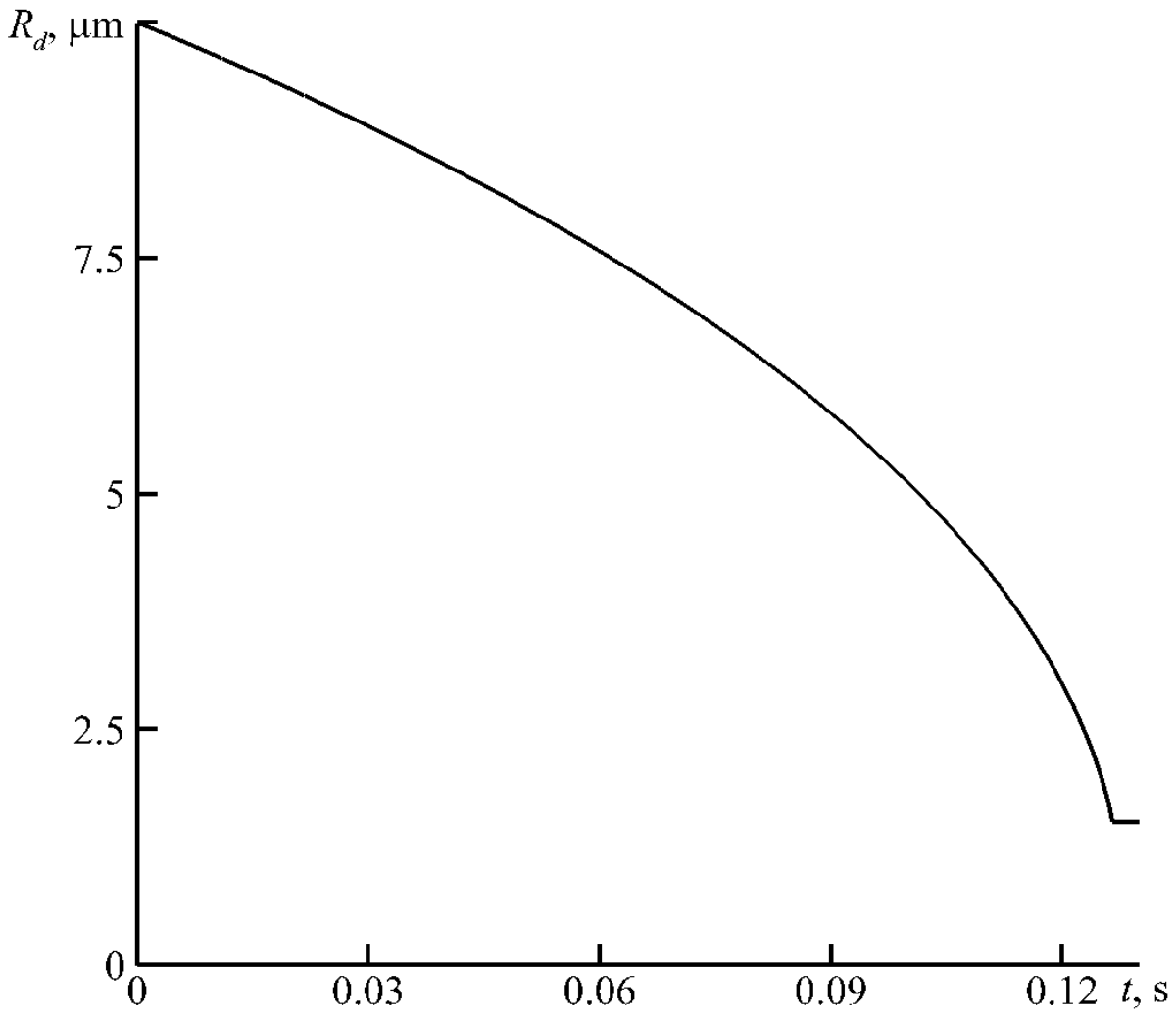

Figure 2

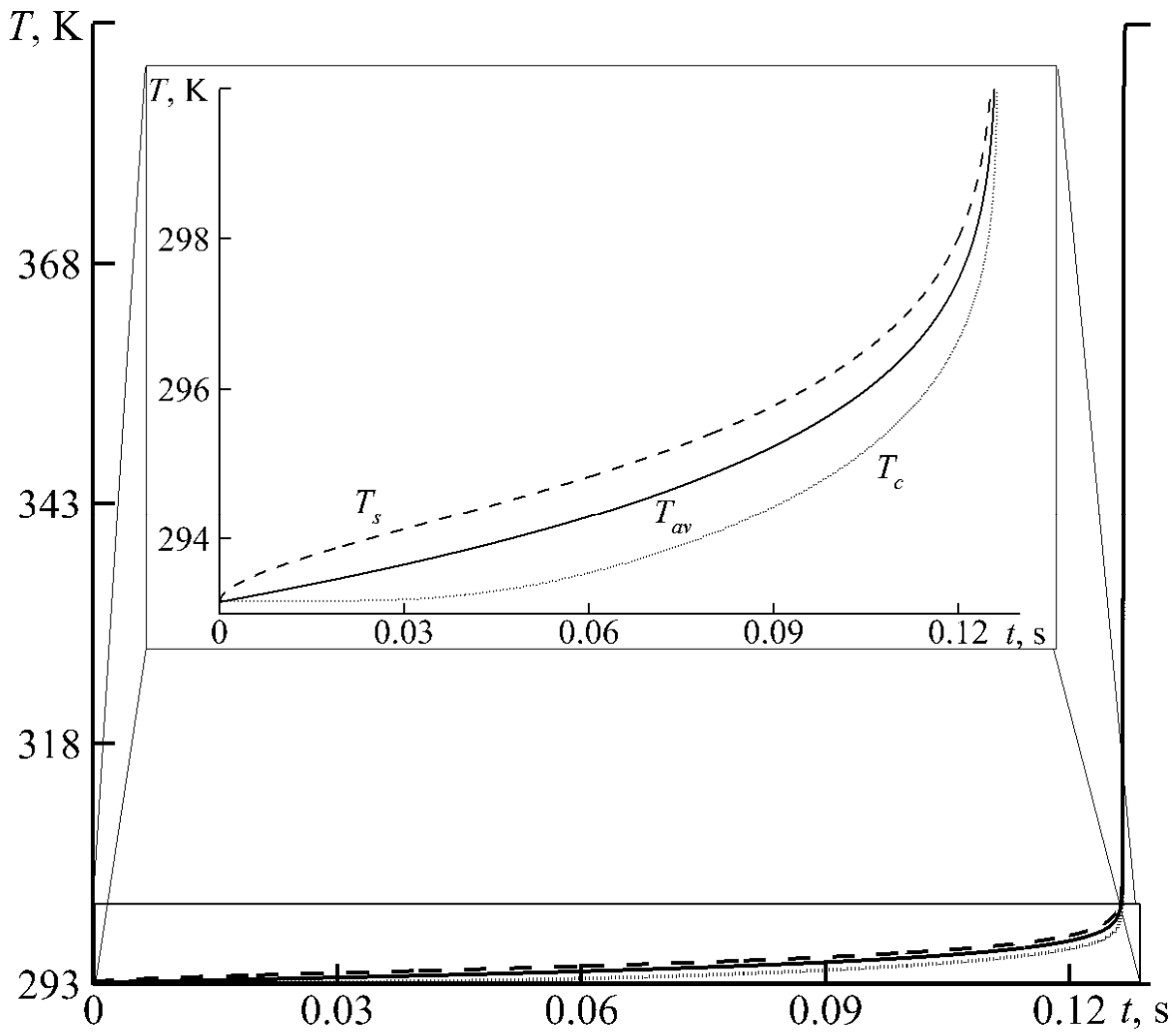
T, K
368
343
318
293
0
0.03
0.06
0.09
0.12 t, s
T, K
298
296
294
0
0.03
0.06
0.09
0.12 t, s
T_s
T_av
T_c

Figure 3

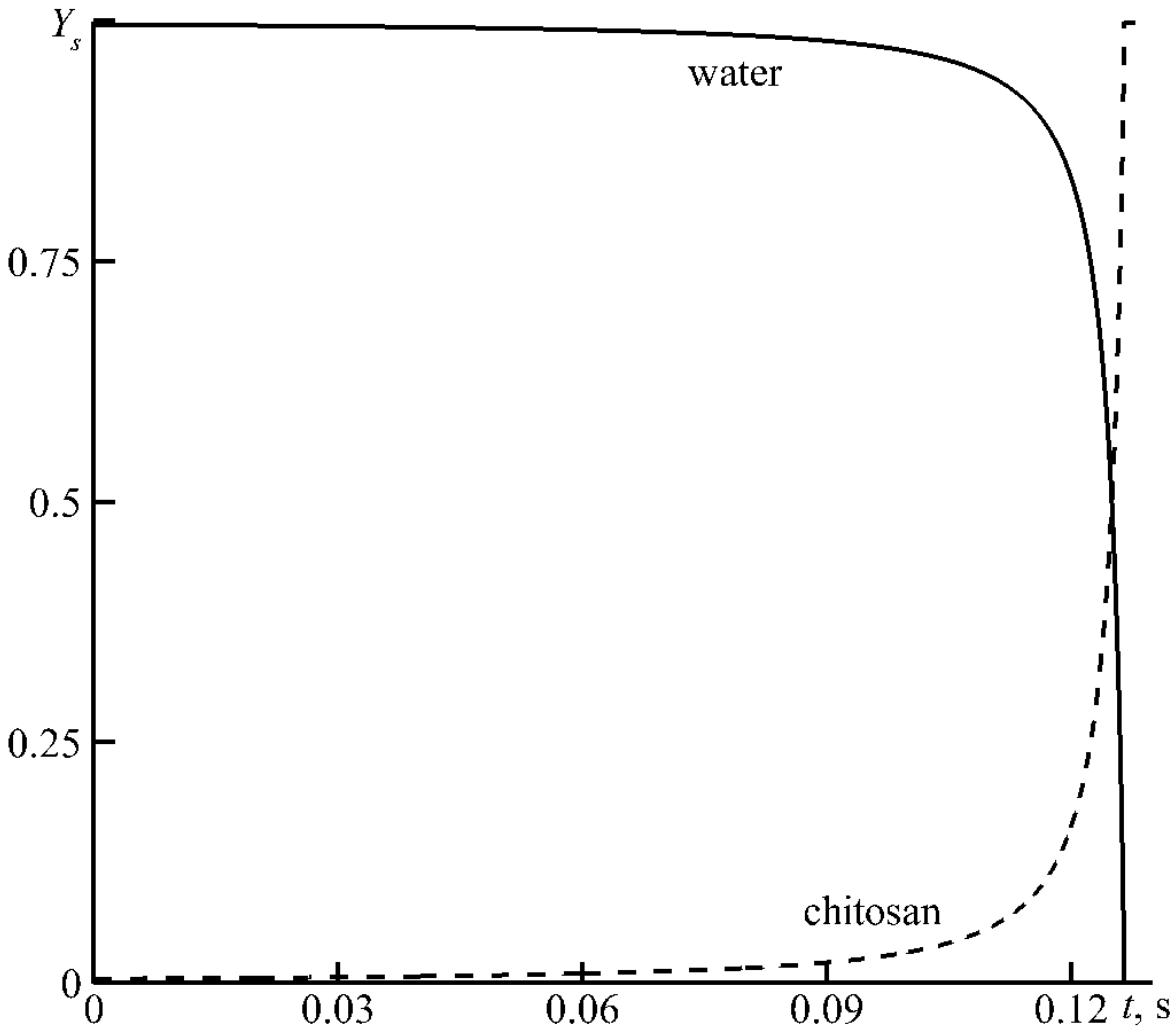

Figure 4